JOURNAL OF CATALYSIS **173,** 95–104 (1998)
ARTICLE NO. CA971922

Mechanistic Studies of the NO–CO Reaction on Rh/Al_2O_3 under Net-Oxidizing Conditions

Steven S. C. Chuang[1] and C.-D. Tan

Department of Chemical Engineering, The University of Akron, Akron, Ohio 44325-3906

Received November 25, 1996; revised August 27, 1997; accepted September 29, 1997

The dynamic behavior of NO and CO adsorbates over a 0.2 wt% Rh/Al_2O_3 catalyst was studied under net-oxidizing conditions by *in situ* infrared spectroscopy combined with pulse transient techniques. The observed sequence of adsorbate and CO_2 concentration profiles during the pulse reaction studies reveals that $Rh^+(CO)_2$ is an active adsorbate which reacts with adsorbed oxygen to form CO_2. The observed transient behaviors of $Rh^+(CO)_2$, $Rh–NO^-$, and CO_2 during the pulse reactions can be explained by the proposed NO–CO reaction mechanism in which (i) $Rh–NO^-$ dissociates to form adsorbed nitrogen and oxygen and (ii) adsorbed oxygen further reacts with $Rh^+(CO)_2$ to produce CO_2. Addition of air to the NO–CO reactant stream produces a net-oxidizing environment for the NO–CO reaction. Adsorbed oxygen from air reacts with $Rh–NO^+$ producing the nitrato species and providing more Rh sites for the NO–CO reaction at 473 K. At 573 K and above, adsorbed oxygen reacts with $Rh^+(CO)_2$ producing CO_2, blocks the reduced Rh^0 sites for $Rh–NO^-$, oxidizes Rh^0/Rh^+ to Rh^{2+} sites, and inhibits the NO conversion and N_2O formation. Rh sites are readily reduced and return to their initial state and the catalyst returns to its initial activity when air is withdrawn from the reactant stream. Preservation of the reduced Rh sites for $Rh–NO^-$ is required to maintain the catalyst activity for the NO–CO reaction under net-oxidizing conditions.

INTRODUCTION

Rhodium has been a major component in the three-way catalytic converter because of its high activity and selectivity for catalyzing the NO–CO reaction. However, the reaction on the Rh catalyst is strongly inhibited by oxygen. The oxygen inhibition effect has limited the use of the Rh-containing three-way catalytic converter to controlling NO emission from the exhaust of stoichiometrically operated engines (1–5). Expanding the operating window or shifting the air to fuel ratio from 14.7 ± 0.3 to greater than 17 (for lean burn and diesel engines) produces an exhaust stream containing excess oxygen, which deactivates Rh catalysts.

The presence of oxygen decreased the activity of Rh for the NO–CO reaction even at a high ratio of carbon monoxide (a reductant) to nitric oxide (an oxidant) (6). The loss of Rh activity may be due to the following: (i) Rh is more active in the $CO–O_2$ reaction than in the NO–CO reaction (7). Excess O_2 rapidly reacts with CO to form CO_2, resulting in low NO conversion and the depletion of reductant CO. (ii) Excess O_2 competes with NO for the adsorption sites and poisons the activity (8). A key step in the NO–CO reaction is the dissociation of NO to form adsorbed N and adsorbed O atoms. This step requires a vacant neighbor site. Site blocking by the adsorbed O atoms may inhibit NO dissociation. (iii) Excess O_2 may deactivate the Rh surface by formation of a near-surface oxide (probably Rh_2O_3) which is catalytically inactive for this reaction (9).

Oxygen in the reactant or exhaust stream that chemisorbs on the Rh surface, forming adsorbed oxygen (10), may affect not only the reactivity of adsorbed NO and CO, but also the Rh surface state. Depending on Rh surface states, CO may chemisorb on the Rh surface in the linear, bridged, and gem-dicarbonyl form; NO may chemisorb as anionic, neutral, cationic, and gem-dinitrosyl form. Transient infrared studies of the NO–CO reaction on Rh/SiO_2 have suggested that anionic NO, $Rh–NO^-$, undergoes dissociation to produce adsorbed nitrogen and adsorbed oxygen atoms (which further react with $Rh^+(CO)_2$ to form CO_2) at 473 and 523 K (i.e., below light-off temperature) (11). Above light-off temperature at 573 K, adsorbed $Rh–NO^-$ and linear CO react to produce CO_2 and N_2. Little is known about the effect of oxygen on the reactivity of the adsorbates during the NO–CO reaction. This paper reports results of a study on the effect of air on NO and CO adsorbates. *In situ* IR spectroscopy was employed to monitor the concentration of adsorbates on the catalyst; mass spectroscopy (MS) was used to determine the composition of the effluents during the pulse transient study of the NO–CO reaction.

EXPERIMENTAL

The Rh/Al_2O_3 catalyst containing 0.2 wt% Rh was prepared by incipient wetness impregnation of $RhCl_3 \cdot 3H_2O$ (Alfa Chemicals) solution onto a γ-alumina support (Alfa Chemicals, 100 m^2/g). The low loading of Rh was used to

[1] To whom correspondence should be addressed.

0021-9517/98 $25.00

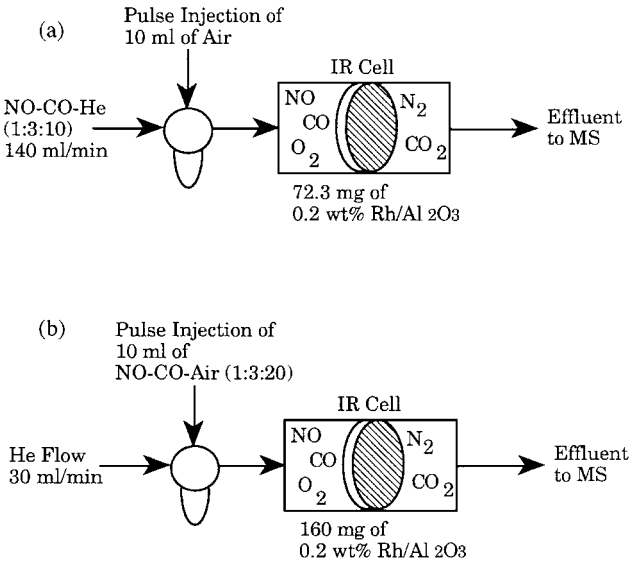

FIG. 1. Schematic diagram of the experimental approaches.

mimic the low content of Rh in the automotive three-way catalyst. The ratio of the volume of solution to the weight of support was 1 cm^3 to 1 g in the impregnation step. After impregnation, the catalyst samples were dried overnight in air at room temperature and reduced in H_2 flow at 673 K for 8 h. The average Rh crystallite size of the 0.2 wt% Rh/Al_2O_3 catalyst was determined to be less than 30 Å by X-ray diffraction (XRD). The number of surface Rh atoms including both Rh^+ and Rh^0 was estimated from the amount of linear CO and gem-dicrabonyl desorbed during temperature-programmed desorption and infrared study. The total number of CO adsorption sites was 29 μmol CO/g catalyst, corresponding to a dispersion of 94%.

An IR reactor cell capable of operating up to 873 K was used for this study (12). The catalysts were pressed into self-supporting disks (13 mg each). One of the disks was placed in the IR reactor cell and the rest were broken down into flakes and placed at the exit line (1/4 in. O.D.) in the immediate vicinity of the infrared beam path to increase the conversion of reactants. A K-type thermocouple (1/16 in. I.D.) was inserted into the IR cell in contact with the catalyst disk.

Figure 1 illustrates the experimental approach which includes (i) pulsing 10 cm^3 of air into a steady-state NO–CO–He (1 : 3 : 10) flow at 140 cm^3/min and (ii) pulsing 10 cm^3 of NO–CO–air (1 : 3 : 20) into a steady-state helium flow at 30 cm^3/min and temperatures between 473 and 633 K and at 0.1 MPa. The specific ratio of the reactant mixture corresponds to that of the exhaust from the lean burn engine at an air to fuel ratio of 18.1 (13). These experiments were aimed at determining the effect of adsorbed oxygen on the dynamic behavior of NO and CO adsorbates as well as the rate of NO conversion and product formation.

The change in the concentration of adsorbates during pulses was monitored by a Fourier transform infrared (FTIR) spectrometer; variation in the effluent gas composition from the IR reactor cell was measured continuously by

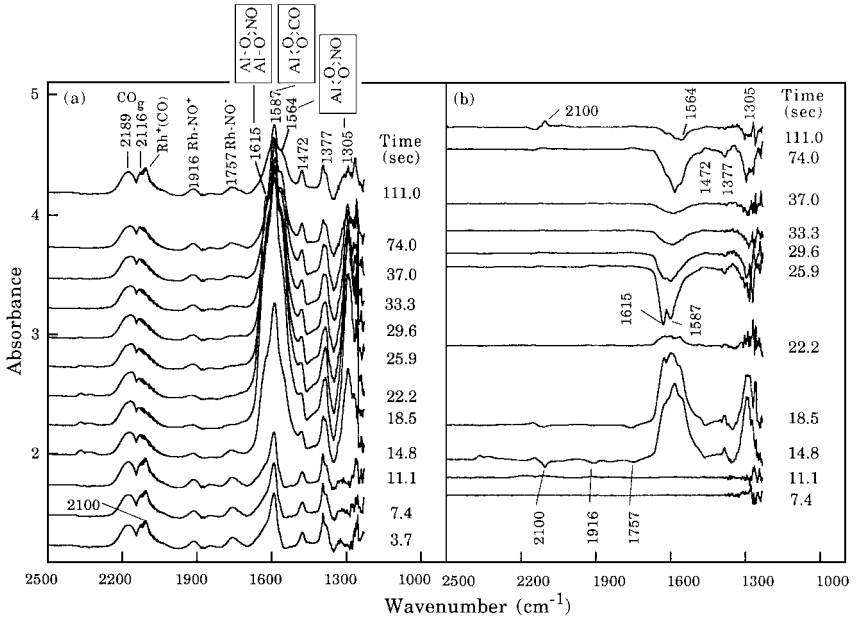

FIG. 2. (a) Transient IR spectra of adsorbates during a 10 cm^3 pulse of air into a flow of NO–CO–He (10 : 30 : 100 cm^3 min^{-1}) at 473 K and 0.1 MPa. (b) The difference spectra between each subsequent spectra (e.g., difference spectrum at 7.4 s is resulted from the difference between the spectra at 7.4 and 3.7 s; difference spectrum at 11.1 s is resulted from the difference between spectra at 11.1 and 7.4 s).

a quadrupole mass spectrometer (MS). The mass-to-charge ratios (*m/e*, i.e., amu) determined by the MS were $m/e = 30$ for NO, $m/e = 46$ for NO_2, $m/e = 32$ for O_2, $m/e = 44$ for N_2O and CO_2, and $m/e = 28$ for N_2 and CO. Separation of the contribution of N_2 and CO to $m/e = 28$ is not possible due to the overlapping of intense secondary *m/e*. The secondary ionization of CO_2 at $m/e = 22$ is used to separate the CO_2 and N_2O contribution to the $m/e = 44$. The ratio of the area under the response curves of $m/e = 44$ and $m/e = 22$ was determined to be 50.8 : 1 ($m/e = 44 : m/e = 22$) from a calibration study injecting a known amount of CO_2 into helium carrier gas. Pulse injection of air, as well as NO–CO–air, limited the amount of oxygen entering the MS chamber, prolonging the lifetime of the MS filament, thereby avoiding frequently shutting down the MS.

RESULTS

Pulse Injection of Air into the NO–CO Flow

The catalyst disk in the IR cell was not subject to any pretreatment prior to the reaction studies in order to emulate the ambient environment of the three-way catalytic converter. Figure 2a shows that exposure of the catalyst to the steady-state NO–CO–He flow at 473 K produced $Rh^+(CO)$ at 2100 cm^{-1}, a Rh–NO^+ band at 1916 cm^{-1}, a high wavenumber Rh–NO^- at 1757 cm^{-1} (14–18), and nitrate/carbonate bands below 1620 cm^{-1} (19). High wavenumber Rh–NO^- denotes adsorbed NO exhibiting an infrared band in the 1740–1770 cm^{-1} region (in contrast to the low wavenumber Rh–NO^- in the 1630–1690 cm^{-1} region) (16–19).

The 10 cm^3 air pulse caused the following changes in the IR intensity of the adsorbates: (i) a decrease in the intensity of $Rh^+(CO)$, Rh–NO^+, and high wavenumber Rh–NO^-, and (ii) an initial increase and then a rapid decrease in the carbonate at 1587 and 1377 cm^{-1} and the nitrate at 1615, 1564, and 1305 cm^{-1} (14, 19). The subtle change in infrared spectra can be further discerned by the sequential difference spectra, shown in Fig. 2b, which highlights the difference between the successive spectra in Fig. 2a. An increase in the coverage of the adsorbate is manifested by the positive band in the difference spectrum; a decrease in the coverage of the adsorbate is manifested by the negative band in the difference spectrum. After air left the reactor, $Rh^+(CO)$, Rh–NO^+, and the high wavenumber Rh–NO^- bands gradually recovered to their initial intensities. Variation of Rh–NO^+ and the high wavenumber Rh–NO^- intensity with time in Fig. 3c clearly shows the slow recovery of the high wavenumber Rh–NO^-, reflecting the slow rate of reduction of oxidized Rh to Rh^0 sites.

Variation in the *m/e* intensity profile in Figs. 3a and 3b shows that the presence of air caused an increase in CO_2 ($m/e = 22$) concentration and a decrease in NO concentration, indicating that the NO conversion was enhanced by the presence of O_2 at 473 K. Further, NO–CO and NO–CO–air pulse reaction studies at 473 K, shown in Table 1, confirm the surprising promotion effect of oxygen on the NO–CO reaction.

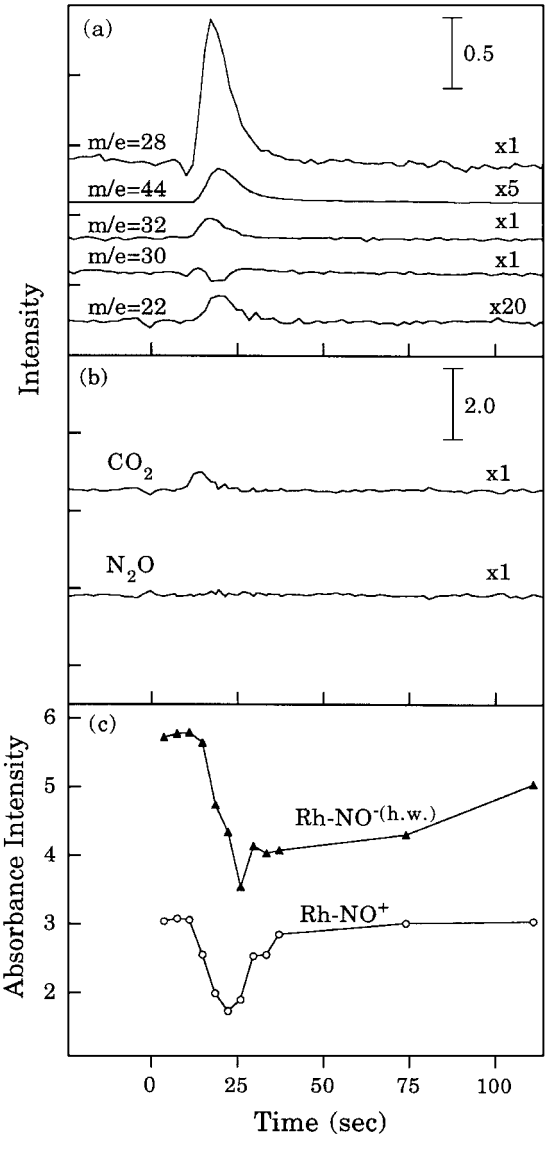

FIG. 3. (a) MS concentration profiles. (b) Concentration profiles of CO_2 and N_2O. (c) Integrated absorbance intensity of adsorbates.

The fifth column in Table 1 lists the NO conversion for the steady-state NO–CO reaction as a function of temperature. The conversion increased from 473 to 573 K and leveled off. At 573 K, exposure of the catalyst to the steady-state NO–CO–He flow shown in Fig. 4a produced $Rh^+(CO)_2$ at 2095 and 2027 cm^{-1}, linear CO on Rh^0 at 2068 cm^{-1}, a weak Rh–NO^+ at 1906 cm^{-1}, high wavenumber Rh–NO^- at 1757 cm^{-1}, carbonate bands at 1587 and 1377 cm^{-1}, and a nitrito band at 1470 cm^{-1}. Al–NCO at 2245 cm^{-1} and Rh–NCO at 2189 cm^{-1} overlapped with N_2O at 2239

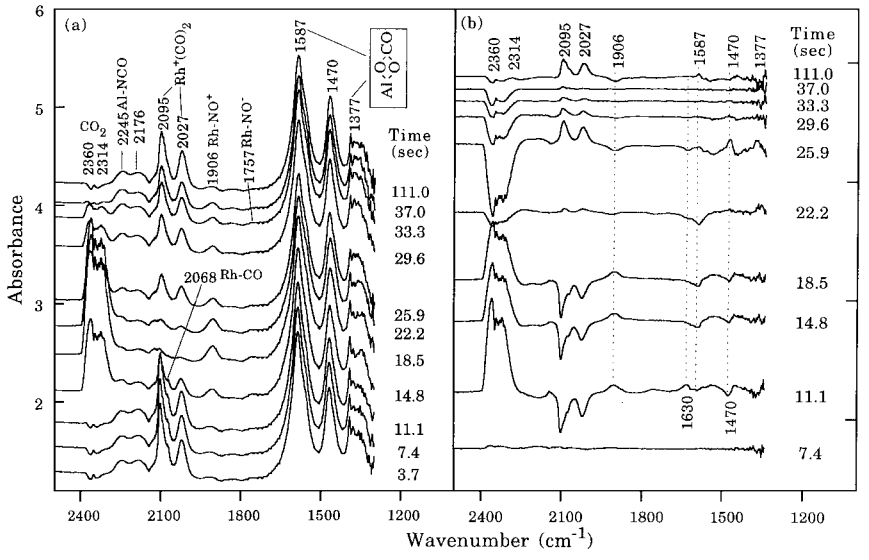

FIG. 4. (a) Transient IR spectra of adsorbates during a 10 cm^3 pulse of air into a flow of NO–CO–He (10 : 30 : 100 cm^3 min^{-1}) at 573 K and 0.1 MPa. (b) The difference spectra between each subsequent spectra.

and 2206 cm^{-1}. The strong and intense band at 2095 cm^{-1} is due to the overlapping of the asymmetric vibration of Rh$^+$(CO)$_2$ with Rh$^+$(CO). The spectral difference in Fig. 4b reveals that the shoulder of the 1587 cm^{-1} band contains a low wavenumber Rh–NO$^-$ at 1630 cm^{-1}.

Figure 4a shows that the air pulse into the NO–CO–He flow caused an increase in the surface concentration of Rh–NO$^+$ and the high wavenumber Rh–NO$^-$, and a decrease in the surface concentration of Rh$^+$(CO), Rh$^+$(CO)$_2$, and the low wavenumber Rh–NO$^-$. The variation of adsorbate coverage can be clearly discerned by the difference in spectra in Fig. 4b. The variation of Rh$^+$(CO)$_2$, Rh–NO$^+$, and CO_2 intensities is also plotted in Fig. 5 to compare with that of gaseous reactant and product concentration. The increase in CO_2 concentration in Fig. 5b indicates the increased rate of CO oxidation while the increased NO concentration in Fig. 5a reflects the reduced rate for NO conversion during the air pulse. The reduced rate of NO conversion appears to result in a low rate of N_2O formation. As air left the IR cell, the adsorbate and the catalyst activity returned to their initial state.

As the reaction temperature rose to 633 K, the NO conversion approached 19% (shown in Table 1) while CO and NO adsorbates on the Rh surface in Fig. 6 show low intensity compared with those at low temperatures. The major IR bands observed during the NO–CO steady-state flow reaction are Al–NCO at 2245 cm^{-1} (20), nitrito at 1470 cm^{-1}, carbonate at 1587 and 1377 cm^{-1}, chelating bidentate nitrato at 1564 cm^{-1}, and Rh–NO$^-$ at 1630 cm^{-1}. The intensities of the bands for adsorbates on Al_2O_3 are considerably greater than those of Rh$^+$(CO)$_2$ at 2095 and 2027 cm^{-1}. The low intensities of the Rh$^+$(CO)$_2$ bands may be attributed to mass transfer control of the overall reaction process. This results in almost complete consumption of reactants near the catalyst pellet surface before reactants enter the pore.

An inset between 2200 and 1800 cm^{-1} in Fig. 6 highlights the effect of air on Rh$^+$(CO)$_2$ and Rh–NO$^+$. The air pulse decreased intensities for all of the IR-observable adsorbates except the carbonate band at 1377 cm^{-1}. The increase in NO concentration at $m/e = 30$ and the decrease in N_2O concentration, shown in Figs. 7a and 7b, indicate that air decreased both NO conversion and N_2O formation. As air left the reactor, N_2O formation immediately recovered to the initial level while Rh–NO$^-$, Rh$^+$(CO)$_2$, and Al–NCO gradually returned to their initial state.

TABLE 1

Conversions Obtained during NO–CO–O_2 and NO–CO–He Pulses on Rh/Al_2O_3 Catalyst[a]

		NO–CO–air			NO–CO–He		
Temperature (K)	Pulses	NO	CO	O_2	NO	NO_{SS}[b]	CO
473	1st	8.8	10.8	24.2	4.1	7.5	5.3
	2nd	8.0	12.2	20.7	3.5		2.7
573	1st	30.3	62.5	16.3	87.2	18.1	26.8
	2nd	35.0	62.5	14.5	90.5		23.1
633	1st	25.1	64.5	38.8	97.3	16.9	32.0
	2nd	32.3	63.2	33.9	96.4		27.6
673	1st	36.3	66.2	43.2	100.0	19.2	33.9
	2nd	32.5	51.9	31.3	100.0	—	26.4

[a] Conversion $X = [(N_A^0 - N_A)/N_A^0] \times 100\%$, where N_A^0 is the moles of A fed to the reactor and N_A is the moles of A leaving the reactor.

[b] NO conversion at steady-state NO–CO–He (10 : 30 : 100 cm^3/min).

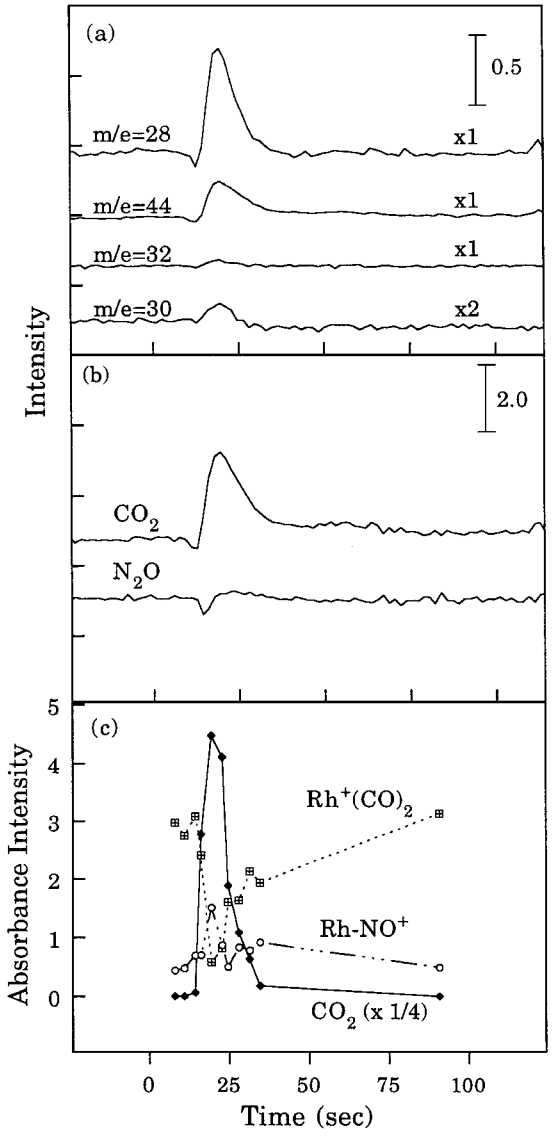

FIG. 5. (a) MS concentration profiles. (b) Concentration profiles of CO_2 and N_2O. (c) Integrated absorbance intensity of adsorbates.

In spite of a strong dependence of the adsorbate intensity on temperature, similar effects of adsorbed oxygen were observed for adsorbates and their reactions at 573 and 633 K. The major effects of adsorbed oxygen are summarized as follows: (i) it decreases the rate of NO conversion and N_2O formation and the intensity of $Rh^+(CO)_2$, (ii) it increases the rate of CO conversion and the intensity of $Rh–NO^+$, and (iii) it inhibits the formation of Rh–NCO and Al–NCO. The significant decrease in $Rh^+(CO)_2$ intensity during the air pulse suggests that adsorbed oxygen either blocks the Rh^+ site for CO adsorption as gem-dicarbonyl (i.e., $Rh^+(CO)_2$) or reacts with gem-dicarbonyl to form CO_2. To further reveal the role of gem-dicarbonyl and adsorbed oxygen in the NO–CO and NO–CO–air reaction, pulse reactions were carried out at 573 K where $Rh^+(CO)_2$ exhibited intense twin bands.

Pulse NO–CO–Air and NO–CO Reactions

Figure 8 compares variation of adsorbate intensities with time during the pulse reaction studies at 573 K. Variations of $Rh^+(CO)_2$, $Rh^{2+}(CO)$, Al–NCO, $Rh–NO^+$, and gaseous CO_2 intensities are plotted along with gaseous reactant and product MS intensities in Fig. 9. Since the catalytic sequence involves adsorption of reactant, conversion of adsorbed reactants to products, and the desorption of adsorbed products, the concentration (i.e., IR intensity) profile of an active adsorbate should lead that of products. Close examination of adsorbate and CO_2 profiles shown in Figs. 9c and 9d shows that $Rh^+(CO)_2$ was the first adsorbate to appear for both reactions; its IR intensity profile paralleled and led that of CO_2 during the pulse NO–CO–air reaction and lagged behind that of CO_2 during the NO–CO reaction. The rapid decrease in $Rh^+(CO)_2$ intensity was followed by an increase in the $Rh–NO^+$ intensity for the NO–CO–air reaction. In contrast, the absence of O_2 allowed the $Rh^+(CO)_2$ intensity to gradually decay as the NO–CO pulse traveled through the catalyst disk. All of these experimental observations point to $Rh^+(CO)_2$ as the active adsorbate participating in the reaction with adsorbed oxygen. In contrast, $Rh^{2+}(CO)$, $Rh–NO^+$, and Al–NCO are the spectator adsorbates whose responses lag behind that of gaseous CO_2 product.

Table 1 compares the conversion of reactants during the pulse NO–CO–air and NO–CO reactions at various temperatures. The observed effect of O_2 on the NO–CO pulse reaction is consistent with those observed for the steady-state

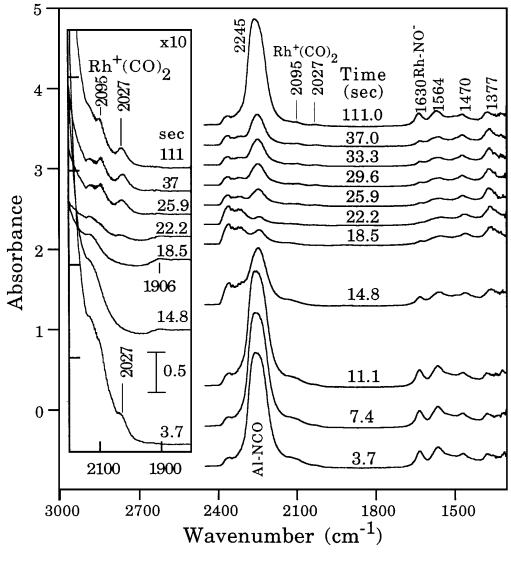

FIG. 6. Transient IR spectra of adsorbates during a 10 cm^3 pulse of air into a flow of NO–CO–He (10 : 30 : 100 cm^3 min^{-1}) at 633 K and 0.1 MPa.

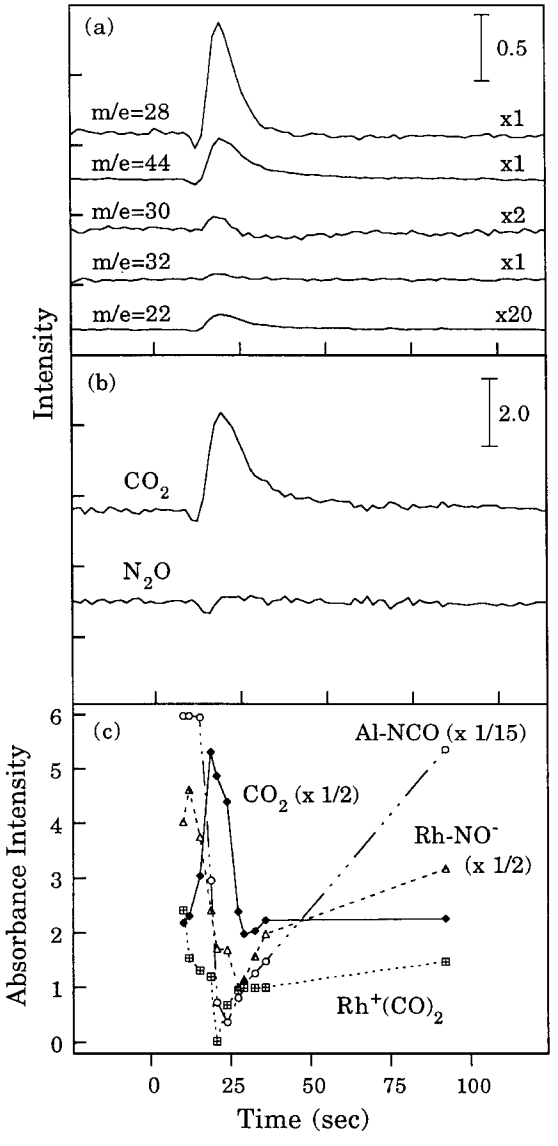

FIG. 7. (a) Corresponding MS analysis of the effluent from the reactor. (b) Concentration profiles of CO_2 and N_2O. (c) Integrated absorbance intensity of adsorbates.

reaction. The presence of O_2 increased the NO conversion at 473 K and decreased the NO conversion at 573 K and above. The absence of O_2 allowed more than 90% NO conversion while the presence of O_2 limited the NO conversion to below 40% at temperatures above 573 K.

DISCUSSION

Reaction Mechanism for NO–CO Reactions on Rh/Al_2O_3

The types of adsorbed NO and CO reflect the state of the Rh surface on which they chemisorb. The observation of $Rh^+(CO)_2$, linear CO on Rh^+ sites [$Rh^+(CO)$], linear CO on Rh^{2+} sites [$Rh^{2+}(CO)$], Rh–NO^+, and Rh–NO^- during the NO–CO reaction indicates that the Rh/Al_2O_3 surface contains both Rh^0 and Rh^+ sites under reaction conditions. Changes in adsorbate and gaseous reactant/product concentration during the pulse and steady-state NO–CO reaction on Rh/Al_2O_3 were found to resemble those observed for the reaction on Rh/SiO_2. The observed sequence of adsorbate and product formation on the Rh surface may be described by the mechanism in Table 2 which has been previously proposed and discussed for the reaction on Rh/SiO_2 (11).

Oxidative disruption (i.e., steps 3 and 4) and reductive agglomeration (step 7) were first proposed by Solymosi and co-workers (21). The rate of these steps was found to be dependent on temperature, Rh crystallite size, and type of support used (11, 21–25). Smaller Rh crystallite size facilitates oxidative disruption and resists reductive agglomeration. Indeed, 4 wt% Rh/SiO_2 catalysts with an average Rh crystallite of 63 Å allowed reductive agglomeration to occur at temperatures above 543 K (11) while 0.2 wt% Rh/Al_2O_3 resisted oxidative disruption even at 673 K. Reductive agglomeration produced the Rh^0 surface which allows the NO–CO reaction to follow the same pathway proposed for the Rh^0 site on the single crystal surface (11).

The major difference between this mechanism and those proposed for the reaction on the Rh single crystal surface is the participation of $Rh^+(CO)_2$ in CO_2 formation. $Rh^+(CO)_2$, which has not been observed on the Rh single crystal surface, was preferentially formed on highly dispersed Rh and/or Rh^+ sites during the NO–CO reaction up to 633 K. The Rh^0 site is the only type of site that has been reported on the Rh single crystal surface for the NO–CO reaction from 253 to 900 K (26–29). The difference in the oxidation state of the Rh site for reaction may explain the large difference in the NO–CO reaction rate on supported and unsupported Rh catalysts (29).

Effect of Air on Reactivity and Dynamics of IR-Observable Adsorbates

The observed effect of air on the NO–CO reaction on Rh/Al_2O_3 is a result of the interactions and reactions of

TABLE 2

Proposed Reaction Mechanism for the NO–CO Reaction

Step 1	$NO_{(g)} + Rh^0 \leftrightarrow Rh^0\text{–}NO^-$
Step 2	$Rh^0\text{–}NO^- + Rh^0 \rightarrow Rh^0\text{–}N + Rh^0\text{–}O$
Step 3	$Rh^0\text{–}NO^- + 2Rh^0 \rightarrow (Rh^+)_2O^{2-} + Rh^0\text{–}N$
Step 4	$Rh^+ + 2CO \leftrightarrow Rh^+(CO)_2$
Step 5	$Rh^+ + NO_{(g)} \leftrightarrow Rh\text{–}NO^+$
Step 6	$Rh\text{–}NO^+ + 2CO_{(g)} \leftrightarrow Rh^+(CO)_2 + NO_{(g)}$
Step 7	$CO_{ad} + (Rh^+)_2O^{2-} \rightarrow 2Rh^0 + CO_2$
Step 8	$Rh^+(CO)_2 + 2O_{ad} \rightarrow Rh^+ + 2CO_2$
Step 9	$Rh^0\text{–}NO^- + Rh^0\text{–}N \rightarrow 2Rh^0 + N_2O_{(g)}$
Step 10	$Rh^0\text{–}N + Rh^0\text{–}N \rightarrow N_{2(g)} + 2Rh^0$
Step 11	$Rh^0\text{–}N + CO_{ad} \rightarrow Rh\text{–}NCO$

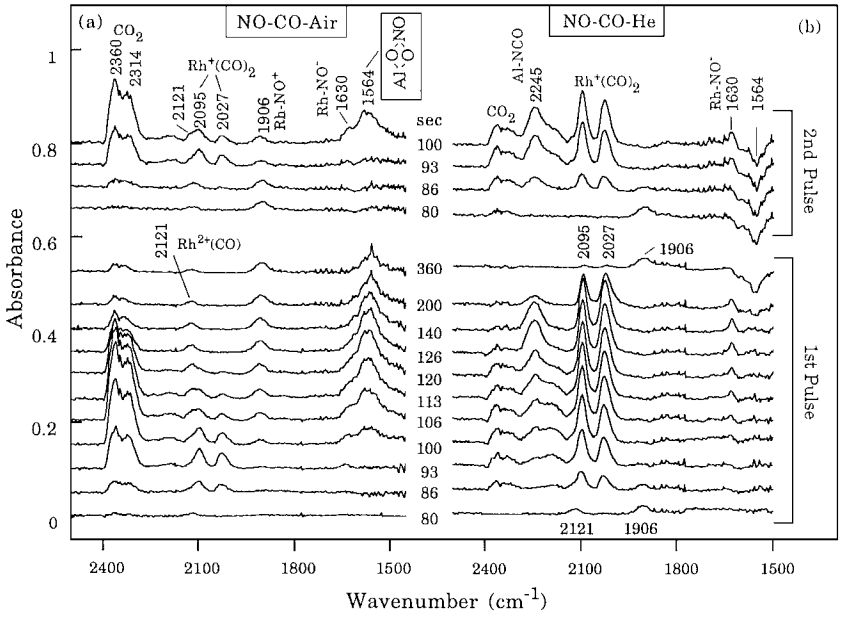

FIG. 8. Transient IR spectra of adsorbates during (a) NO–CO–air and (b) NO–CO–He pulses at 573 K and 0.1 MPa.

adsorbed oxygen with adsorbed NO and adsorbed CO. Direct spectroscopic observation of adsorbed oxygen, NO, and CO would allow unambiguous identification of the role of adsorbed oxygen in the NO–CO reaction. Unfortunately, infrared spectra of adsorbed oxygen cannot be obtained from this study due to cutoff of the IR transmission by the Al_2O_3 support at 1150 cm^{-1} and below. The interactions and reactions of adsorbed oxygen with adsorbed NO and CO have to be elucidated by variation of NO and CO adsorbates during the addition of air to the NO–CO reaction.

Table 3 summarizes the effect of air (i.e., adsorbed oxygen) on the surface concentration of IR-observable adsorbates. An interesting effect, adsorbed oxygen promotion of NO conversion, may be attributed to the removal of adsorbed oxygen by the reaction of $Rh–NO^+$ with adsorbed oxygen, forming nitrato species:

$$Rh–NO^+ + 2O_{ad} \leftrightarrow (NO_3)_{ad} + Rh^+.$$

The nitrato species appears to decompose back to $Rh–NO^+$ when gaseous oxygen leaves the reactor. The occurrence of this reaction step is supported by the increase in intensity of nitrato species with a concomitant decrease in $Rh–NO^+$ intensity at 473 K, shown in Fig. 2. This reaction would allow removal of adsorbed oxygen without consuming reducing agent (i.e., CO), facilitating dissociation of high wavenumber $Rh–NO^-$, and thus enhancing NO conversion. Further study is required to determine whether promotion of NO conversion by air at 473 K ceases when nitrato species is saturated on the catalyst surface.

TABLE 3

Effect of Air on the Surface Concentration of IR-Observable Adsorbates[a]

Adsorbates	473 K	573 K	633 K	673 K
Low wavenumber $Rh–NO^-$	NA	–	–	–
High wavenumber $Rh–NO^-$	–	+	NA	NA
$Rh–NO^+$	–	+	+	+
$Rh^+(CO)_2$	NA	–	–	–
$Rh^+(CO)$	–	–	NA	NA
Carbonate (CO_3^{2-})	+	NA	NA	NA
Nitrate (NO_3^-)	+	NA	–	NA
Rh–NCO	NA	–	NA	NA
Al–NCO	NA	–	–	–
Rate of NO conversion	+	–	–	–

[a] (–) decrease, (+) increase, (NA) not available.

The effect of adsorbed oxygen on the nitrato species is less obvious at 573 K than at 473 K. The role of adsorbed oxygen in the NO–CO reaction at 573 K may be revealed by comparing the concentration profiles of adsorbates and gaseous CO_2 products in Figs. 4 and 5. Two fundamental questions that can be addressed by these profiles are how adsorbed oxygen inhibits the NO conversion and whether $Rh^+(CO)_2$ participates in CO_2 formation.

Table 2 suggests that the first step of the NO–CO reaction is the dissociation of the low wavenumber $Rh–NO^-$. $Rh–NO^-$ is an anionic NO species formed by the transfer of a partial charge from the reduced Rh to the antibonding orbital of adsorbed NO^-; the $Rh–NO^-$ as a whole should be considered a neutral species (11). The rationale for $Rh–NO^-$ dissociation is that a great amount of electron transfer from the reduced Rh surface to the antibonding orbital of adsorbed NO shifts $Rh–NO^-$ to a low wavenumber

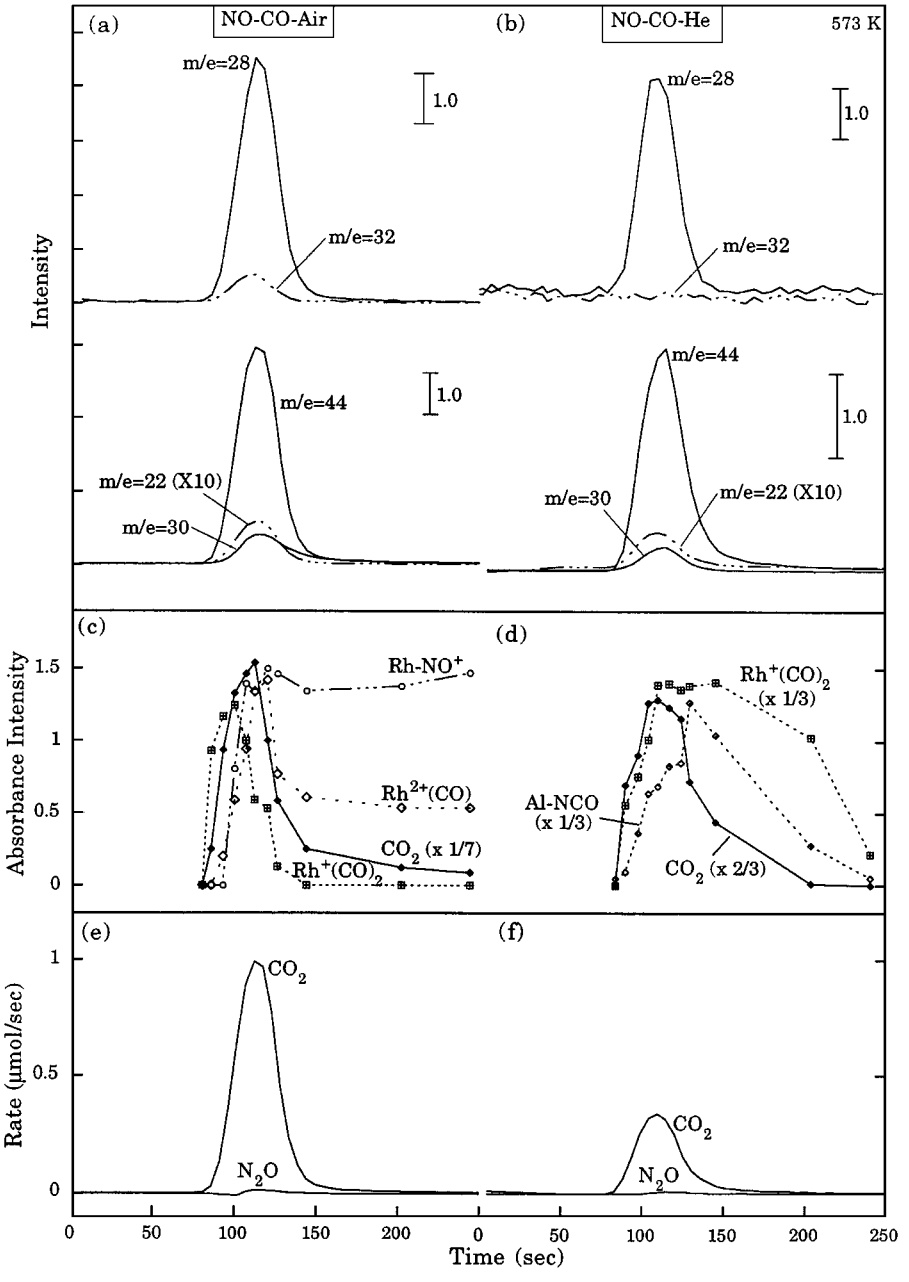

FIG. 9. MS analysis of the effluent from the reactor, integrated absorbance intensity of adsorbates, and formation rates of CO_2 and N_2O during the NO–CO–air pulse, (a), (c), (e) and NO–CO–He pulse, (b), (d), (f) in Fig. 8.

and results in a weakening of the N–O bond and a strengthening of the Rh–N bond (11, 17). This suggests that the low wavenumber Rh–NO^- may be the precursor for NO dissociation.

As listed in Table 2, the reaction steps involved with Rh-NO^- can be expressed in the form of the consecutive and parallel reactions

$$\mathrm{NO} + \mathrm{Rh}^0 \underset{r_{-1}}{\overset{r_{+1}}{\rightleftharpoons}} \mathrm{Rh{-}NO}^- \overset{\begin{matrix}\mathrm{Rh}^0 r_2 \\ 2\mathrm{Rh}^0 r_3\end{matrix}}{\begin{matrix}\longrightarrow \\ \longrightarrow\end{matrix}} \begin{matrix}\mathrm{Rh}^0{-}\mathrm{N} + \mathrm{Rh}^0{-}\mathrm{O} \\ (\mathrm{Rh}^+)_2\mathrm{O}^{2-} + \mathrm{Rh}^0{-}\mathrm{N}\end{matrix},$$

where r_{+1} is the rate of NO adsorption, r_{-1} is the rate of NO desorption, and r_2 and r_3 are the rates of NO dissociation. Since Rh–NO^- is the intermediate in the consecutive reaction pathway, the intensity of Rh–NO^- should be proportional to $r_{+1}/(r_{-1}+r_2+r_3)$. A decrease in NO conversion reflects the decrease in r_2 and r_3; a decrease in Rh–NO^- intensity further suggests that the decrease in r_{+1} is more than that in r_2 and r_3. Thus, the low NO conversion rate (r_2+r_3) and Rh–NO^- intensity in the NO–CO–air reaction when compared with those in the NO–CO reaction may be ascribed to a decrease in reduced Rh sites for NO

adsorption through either (i) the blocking of $Rh–NO^-$ sites by adsorbed oxygen or (ii) the oxidation of Rh^0 to Rh^+/Rh^{2+} sites.

Removal of adsorbed oxygen from both dissociated NO and O_2 is required to sustain the catalytic cycle of the NO–CO reaction in either the reductive or the oxidizing environment. Adsorbed oxygen from dissociated NO has been shown to react with $Rh^+(CO)_2$ to produce CO_2 during the NO–CO reaction (11). The reaction of adsorbed oxygen from O_2 with $Rh^+(CO)_2$ was demonstrated in Fig. 9c, which shows the $Rh^+(CO)_2$ profile leading that of CO_2 during the NO–CO–air pulse reaction. The lead–lag relation between $Rh^+(CO)_2$ and CO_2 followed the sequence of adsorbate to product as discussed in the previous section. Further evidence for this reaction is the rapid decrease in $Rh^+(CO)_2$ intensity accompanied by an increase in CO_2 formation during the air pulse into the NO–CO flow shown in Fig. 5c. Depletion of $Rh^+(CO)_2$ by reaction with adsorbed oxygen during the air pulse produced free Rh^+ sites for NO adsorption as $Rh–NO^+$. These proposed steps explain the inverse relationship between $Rh^+(CO)_2$ and $Rh–NO^+$ coverage, shown in Figs. 5c and 9c, clearly showing that one of the effects of adsorbed oxygen is to keep part of the Rh surface in an oxidizing state which adsorbs $Rh^+(CO)_2$ and $Rh–NO^+$. Adsorbed oxygen also oxidizes part of Rh to form a Rh^{2+} site as evidenced by the persistence of the $Rh^{2+}(CO)$ band at 2121 cm^{-1} which followed the $NO–CO–O_2$ pulse reaction shown in Fig. 8a. The delayed response of $Rh^{2+}(CO)$ with respect to that of gaseous CO_2 product in Fig. 9 indicates that $Rh^{2+}(CO)$ is a spectator which is not involved in the catalytic sequence of CO_2 formation, further suggesting that Rh^{2+} is inactive for the NO–CO reaction.

Isocyanate species (NCO) on Rh and Al_2O_3 surfaces, which were produced from the NO–CO reaction, were consumed during the air pulse into the NO–CO flow and were inhibited by adsorbed oxygen during the pulse NO–CO–air reaction. Since both adsorbed NCO and gaseous N_2O formation require adsorbed N from dissociated NO, inhibition of their formation can be attributed to poisoning of the NO dissociation site by adsorbed oxygen.

CONCLUSIONS

The mechanism of the NO–CO reaction under net-oxidizing conditions over a 0.2 wt% Rh/Al_2O_3 catalyst has been studied by *in situ* infrared spectroscopy combined with pulse transient techniques. Dynamic behavior of adsorbates and product formation during the pulse reaction allows identification of spectator and active adsorbates. The observed sequence of adsorbate and CO_2 concentration profiles reveals that $Rh^+(CO)_2$ is an active adsorbate which reacts with adsorbed oxygen to form CO_2; $Rh^{2+}(CO)$, $Rh–NO^+$, and Al–NCO are the spectator adsorbates whose responses (i.e., concentration profiles) lag significantly behind that of gaseous CO_2 product. The observed transient behaviors of $Rh^+(CO)_2$, $Rh–NO^-$, and CO_2 can be explained by the proposed NO–CO reaction mechanism in which (i) $Rh–NO^-$ dissociates to form adsorbed nitrogen and oxygen and (ii) adsorbed oxygen further reacts with $Rh^+(CO)_2$ to produce CO_2.

Addition of air to the NO–CO reactant stream produces a net oxidizing environment for the NO–CO reaction. Adsorbed oxygen from air reacts with $Rh–NO^+$, producing the nitrato species and providing more Rh sites for NO–CO reaction at 473 K. At 573 K and above, adsorbed oxygen reacts with $Rh^+(CO)_2$ producing CO_2, blocks the reduced Rh^0 site for $Rh–NO^-$, oxidizes Rh^0/Rh^+ to Rh^{2+} sites, and inhibits the NO conversion and N_2O formation. Rh sites are readily reduced and return to their initial state and the catalyst returns to its initial activity when air is withdrawn from the reactant stream. Preservation of the reduced Rh sites for $Rh–NO^-$ is required to maintain the catalyst activity for the NO–CO reaction under net-oxidizing conditions.

ACKNOWLEDGMENT

Although the research described in this article has been funded wholly by the United States Environmental Protection Agency under assistance agreement R823529-01-0 to the University of Akron, it has not been subjected to the Agency's peer and administrative review and therefore may not necessarily reflect the views of the Agency and no official endorsement should be inferred.

REFERENCES

1. Shelef, M., and Graham, G. W., *Catal. Rev. Sci. Eng.* **36**, 433 (1994).
2. Iwamoto, M., *in* "Future Opportunities in Catalytic and Separation Technology" (M. Misono, Y. Moro-oka, and S. Kimura, Eds.), p. 121. Elsevier, Amsterdam/Oxford/New York/Tokyo, 1990.
3. Taylor, K. C., *Catal. Rev. Sci. Eng.* **35**, 457 (1993).
4. Summers, J. C., and Williamson, W. B., *in* "Environmental Catalysis" (J. N. Armor, Ed.), ACS Symposium Series, Vol. 552, p. 96. Am. Chem. Soc., Washington, DC, 1994.
5. Tamaru, K., and Mills, G. A., *in* "Catalysts for Control of Exhaust Emissions," Adv. Heterogeneous Catalyst for Energy Application, Chapter 8. DE-FG02-92ER30201, U.S. Department of Energy, 1994.
6. Taylor, K. C., and Schlatter, J. C., *J. Catal.* **63**, 53 (1989).
7. Oh, S. H., and Carpenter, J. E., *J. Catal.* **101**, 114 (1986).
8. Iwamoto, M., and Hamada, H., *Catal. Today* **10**, 57 (1991).
9. Peden, C. H. F., Goodman, D. W., Blair, D. S., Berlowitz, P. J., Fisher, G. B., and Oh, S. H., *J. Phys. Chem.* **92**, 1563 (1988).
10. Boreskov, G. K., *in* "Catalysis Science and Technology" (J. R. Anderson and M. Boudart, Eds.). Springer-Verlag, New York, 1982.
11. Krishnamurthy, R., and Chuang, S. S. C., *J. Phys. Chem.* **99**, 16727 (1995).
12. Chuang, S. S. C., Brundage, M. A., Balakos, M. W., and Srinivas, G., *Appl. Spectrosc.* **49**, 1151 (1995).
13. Kharas, K. C. C., *Appl. Catal. B* **2**, 207 (1993).
14. Davydov, A. A., *in* "Infrared Spectroscopy of Adsorbed Species on the Surface of Transition Metal Oxides" (C. H. Rochester, Ed.), Wiley, Chichester, 1990.
15. Arai, H., and Tominaga, H., *J. Catal.* **43**, 131 (1976).
16. Srinivas, G., Chuang, S. S. C., and Debnath, S., *J. Catal.* **148**, 748 (1994).

17. Hecker, W. C., and Bell, A. T., *J. Catal.* **85**, 389 (1984).
18. Chuang, S. S. C., and Tan, C.-D., *Catal. Today* **35**, 369 (1996).
19. Nakamoto, K., "Infrared and Raman Spectra of Inorganic and Coordination Compounds," 4th ed. Wiley, New York, 1986.
20. Solymosi, F., and Sarkany, J., *Appl. Surf. Sci.* **3**, 68 (1979).
21. Solymosi, F., and Pasztor, M., *J. Phys. Chem.* **89**, 4789 (1985).
22. Basu, P., Panayotov, D., and Yates, J. T., Jr., *J. Am. Chem. Soc.* **110**, 2074 (1988).
23. Solymosi, F., Bansagi, T., and Novak, E., *J. Catal.* **112**, 183 (1988).
24. Novak, E., Sprinceana, D., and Solymosi, F., *App. Catal. A: Gen.* **149**, 89 (1997).
25. Van't Blick, H. F. J., Van Zon, J. B. A. D., Huizinga, T., Vis, J. C., Koningsberger, D. C., and Prins, R., *J. Am. Chem. Soc.* **107**, 3139 (1985).
26. Peden, C. H. F., and Herman, G. S., *in* "15th Meeting of the North American Catalysis Society, Chicago, 1997."
27. Root, T. W., Fisher, G. B., and Schmidt, L. D., *J. Chem. Phys.* **85**, 4687 (1986).
28. Belton, D. N., DiMaggio, C. L., Schmieg, S. J., and Ng, K. Y. S., *J. Catal.* **157**, 559 (1995).
29. Oh, S. H., Fisher, G. B., Carpenter, J. E., and Goodman, D. W., *J. Catal.* **100**, 360 (1986).